SCIENTIFIC REPORTS

OPEN

Quantum magnetisms in uniform triangular lattices $Li_2AMo_3O_8$ (A = In, Sc)

Received: 19 June 2018
Accepted: 7 November 2018
Published online: 12 February 2019

Kazuki Iida[1], Hiroyuki Yoshida[2], Hirotaka Okabe[3], Naoyuki Katayama[4], Yuto Ishii[2], Akihiro Koda[3,5], Yasuhiro Inamura[6], Naoki Murai[6], Motoyuki Ishikado[1], Ryosuke Kadono[3,5] & Ryoichi Kajimoto[6]

Molecular based spin-1/2 triangular lattice systems such as $LiZn_2Mo_3O_8$ have attracted research interest. Distortions, defects, and intersite disorder are suppressed in such molecular-based magnets, and intrinsic geometrical frustration gives rise to unconventional and unexpected ground states. $Li_2AMo_3O_8$ (A = In or Sc) is such a compound where spin-1/2 Mo_3O_{13} clusters in place of Mo ions form the uniform triangular lattice. Their ground states are different according to the A site. $Li_2InMo_3O_8$ undergoes conventional 120° long-range magnetic order below $T_N = 12$ K whereas isomorphic $Li_2ScMo_3O_8$ exhibits no long-range magnetic order down to 0.5 K. Here, we report exotic magnetisms in $Li_2InMo_3O_8$ and $Li_2ScMo_3O_8$ investigated by muon spin rotation (μSR) and inelastic neutron scattering (INS) spectroscopies using polycrystalline samples. $Li_2InMo_3O_8$ and $Li_2ScMo_3O_8$ show completely different behaviors observed in both μSR and INS measurements, representing their different ground states. $Li_2InMo_3O_8$ exhibits spin wave excitation which is quantitatively described by the nearest neighbor anisotropic Heisenberg model based on the 120° spin structure. In contrast, $Li_2ScMo_3O_8$ undergoes short-range magnetic order below 4 K with quantum-spin-liquid-like magnetic fluctuations down to the base temperature. Origin of the different ground states is discussed in terms of anisotropies of crystal structures and magnetic interactions.

When quantum spins are aligned on geometrically frustrated lattices, unusual ground state eventually emerges among energetically competed states[1–3]. Two-dimensional (2D) spin-1/2 triangular lattice Heisenberg antiferromagnet (TLHAF) is a prototypical system of geometrically frustrated magnets. Theoretically, the ground states of 2D TLHAF with both quantum and classical spins are known to be so-called 120° long-range order[4–7]. When perturbations such as the second nearest-neighbor interaction[8], ring exchange interaction[9], spatially anisotropic interactions[10], and randomness of the strength of the nearest-neighbor interaction[11] are set in, the system undergoes a quantum spin liquid (QSL) ground state where the system does not show static long-range magnetic order but shows long-range entanglement and fractional excitations[1,2]. Extensive experimental studies have also been conducted on spin-1/2 TLHAFs; the 120° long-range magnetic order is reported in $Ba_3CoSb_2O_9$[12–14] whereas QSL state is proposed for the ground states of κ-$(BEDT\text{-}TTF)_2Cu_2(CN)_3$[15,16], $EtMe_3Sb[Pd(dmit)_2]_2$[17,18], $YbMgGaO_4$[19–22] and 1T-TaS_2[23]. Furthermore, spin-1 TLHAF $Ba_3NiSb_2O_9$ also shows QSL behaviors[24–26]. QSL with spinon Fermi surface[27,28] was proposed and succeeded in understanding the QSL behaviors in such compounds[20,21,26]. However, experimental realization of the QSL ground state in spin-1/2 TLHAF systems is still limited and remains an intriguing pursuit.

Recently, cluster magnet $LiZn_2Mo_3O_8$ has attracted considerable research interest as spin-1/2 TLHAF[29]. Seven 4d electrons in a Mo_3O_{13} cluster occupy their orbitals, resulting in one unpaired electron. Unpaired electron with spin $S = 1/2$ remains in the total symmetry of the Mo_3O_{13} cluster (A_1 irreducible representation) with equal contributions from all three Mo atoms, and network of the magnetic clusters forms a uniform triangular lattice

[1]Neutron Science and Technology Center, Comprehensive Research Organization for Science and Society (CROSS), Tokai, Ibaraki, 319-1106, Japan. [2]Department of Physics, Faculty of Science, Hokkaido University, Sapporo, Hokkaido, 060-0810, Japan. [3]Institute of Materials Structure Science, High Energy Accelerator Research Organization (KEK), Tokai, Ibaraki, 319-1106, Japan. [4]Department of Applied Physics, Nagoya University, Nagoya, Aichi, 464-8603, Japan. [5]Department of Materials Structure Science, Sokendai (The Graduate University for Advanced Studies), Tsukuba, Ibaraki, 305-0801, Japan. [6]J-PARC Center, Japan Atomic Energy Agency (JAEA), Tokai, Ibaraki, 319-1195, Japan. Correspondence and requests for materials should be addressed to K.I. (email: k_iida@cross.or.jp)

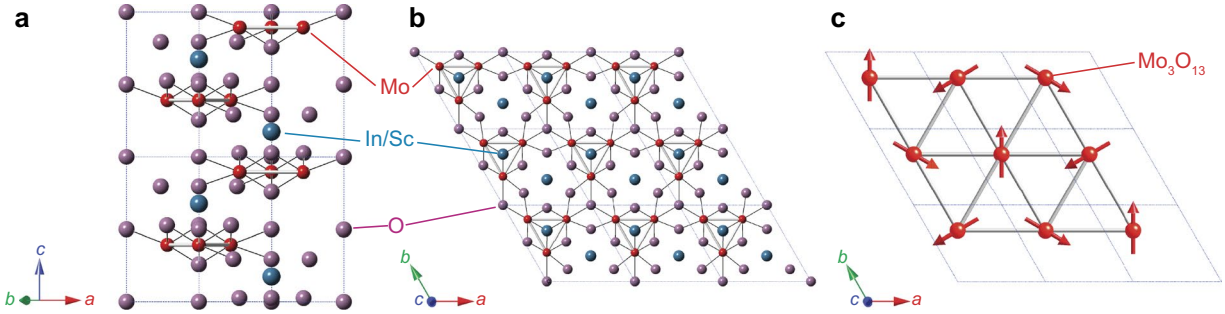

Figure 1. (**a**,**b**) Crystal structure of $Li_2AMo_3O_8$. Li site is not depicted. (**c**) 120° spin structure on the Mo_3O_{13}-based triangular lattice in $Li_2InMo_3O_8$. Dashed lines in each panel represent the chemical unit cell.

in $LiZn_2Mo_3O_8$. The dominant magnetic interaction between spin-1/2 Mo_3O_{13} clusters is antiferromagnetic[29], yielding geometrical frustration. $LiZn_2Mo_3O_8$ is therefore an ideal 2D spin-1/2 TLHAF system. Magnetic susceptibility and heat capacity measurements suggested that 2/3 of $S = 1/2$ spins are quenched below 96 K, and condensed valence bond state (VBS) where resonance valence-bond states[30,31] coexist with remnant paramagnetic spins is proposed for the possible ground state[29,32]. Gapless spin excitations were reported by electron spin resonance[32], ^{7}Li nuclear magnetic resonance (NMR)[32], muon spin rotation (μSR)[32], and inelastic neutron scattering (INS)[33] measurements. Emergent honeycomb lattice is theoretically proposed for the origin of the condensed VBS[34]. Recently, a 1/6-filled extended Hubbard model in an anisotropic kagome lattice is also proposed to account for the low temperature phase of $LiZn_2Mo_3O_8$[35]. However, intersite disorder between Li^+ and Zn^{2+} ions is reported[29,32], which may affect on the intrinsic magnetism in $LiZn_2Mo_3O_8$.

New molecular based triangular lattice systems $Li_2AMo_3O_8$ where A = In or Sc are of particular interest in this context[36,37]. $Li_2AMo_3O_8$ crystallizes in a hexagonal structure $P6_3mc$, and no intersite disorder between Li^+ and A^{3+} sites exists (see Supplementary Information). As in $LiZn_2Mo_3O_8$, spin-1/2 carrying Mo_3O_{13} clusters are arranged on the structurally perfect triangular lattice separated by nonmagnetic Li and A layers in both compounds as shown in Fig. 1(a,b). Susceptibility measurements of both compounds report that the dominant magnetic interactions are antiferromagnetic and the effective moments are 1.61 μ_B (In) and 1.65 μ_B (Sc), which are close to $p_{eff} = 1.73\ \mu_B$ the ideal value for spin $S = 1/2$. Spin-1/2 TLHAF is therefore realized in $Li_2AMo_3O_8$, whose ground states are however different from each other. In $Li_2InMo_3O_8$, long-range magnetic order develops below $T_N = 12$ K with Curie-Weiss temperature of $\Theta_{CW} = -242$ K, and ^{7}Li NMR study suggests that the magnetic structure is the 120° structure as described in Fig. 1(c). On the other hand, isostructural $Li_2ScMo_3O_8$ shows no long-range magnetic order down to 0.5 K in spite of large Weiss temperature of $\Theta_{CW} = -127$ K. Instead, both magnetic susceptibility and heat capacity measurements indicate the development of short-range magnetic order below 10 K. Spin glass state is ruled out as the ground state of $Li_2ScMo_3O_8$ since the magnetic susceptibility shows no splitting between zero-field-cooling and field-cooling processes[37]. Low-temperature heat capacity measurements in $Li_2ScMo_3O_8$ shows sizable T-linear term $\gamma_{mag} = 35.7\ mJ/mol \cdot K^2$, which is similar to those of QSL candidates κ-$(BEDT\text{-}TTF)_2Cu_2(CN)_3$[16], $EtMe_3Sb[Pd(dmit)_2]_2$[18], and $Ba_3CuSb_2O_9$[38]. Furthermore, different magnetic entropies between $Li_2ScMo_3O_8$ and $LiZn_2Mo_3O_8$ suggests that the ground state in $Li_2ScMo_3O_8$ is QSL rather than condensed VBS. Because of easy access to two different ground states of spin-1/2 TLHAF, $Li_2AMo_3O_8$ is an intriguing system to investigate 2D spin-1/2 TLHAF. However, lack of microscopic measurements prevents us from fully understanding the ground states and dynamics of $Li_2AMo_3O_8$. In this paper, we investigate quantum magnetisms of polycrystalline $Li_2InMo_3O_8$ and $Li_2ScMo_3O_8$ by combination of μSR and time-of-flight (TOF) neutron scattering techniques.

Results and Discussion

Zero field- (ZF-) μSR time spectra of $Li_2InMo_3O_8$ at several temperatures are shown in Fig. 2(a). The spectra show a damping at around 12 K, and spectral oscillations appear at lower temperatures. It is a direct evidence of the long-range magnetic order as reported in the earlier studies[36,37,39,40]. Fourier transform of the spectrum at 3.33 K [see the inset of Fig. 2(a)] suggests that at least three different local fields are found in $Li_2InMo_3O_8$, which is probably due to crystallographically inequivalent muon stopping sites indicated by our density functional theory (DFT) calculation (see Supplementary Fig. S3 for $Li_2ScMo_3O_8$). The ZF-μSR spectra of $Li_2InMo_3O_8$ are fitted by three cosine functions with transverse and longitudinal relaxations

$$A_{ZF}(t) = \sum_{n=1}^{3} A_n \left[\frac{2}{3} \cos(2\pi f_n t + \phi) \exp(-\lambda_t t) + \frac{1}{3} \exp(-\lambda_l t) \right] + A_{BG} \quad (1)$$

where A_n and A_{BG} are the positron decay asymmetries of each oscillation ($n = 1$~3) and background (mainly from a silver backing plate) components, f_n is the precession frequency, ϕ is the initial phase, and λ_t (λ_l) is the transverse (longitudinal) relaxation rate. Fitting result at each temperature is shown in Fig. 2(a). Local magnetic fields of 84.9(3), 103.1(2), and 151.5(5) G are extracted at 3.33 K, and these values are comparable in magnitude of local fields that are observed in spin-1/2 magnets[41]. Figure 2(c) shows temperature dependences of f_1, f_2, and f_3, representing that long-range magnetic order evolves in $Li_2InMo_3O_8$ below $T_N = 12$ K with the critical exponents $\beta \sim 0.33$.

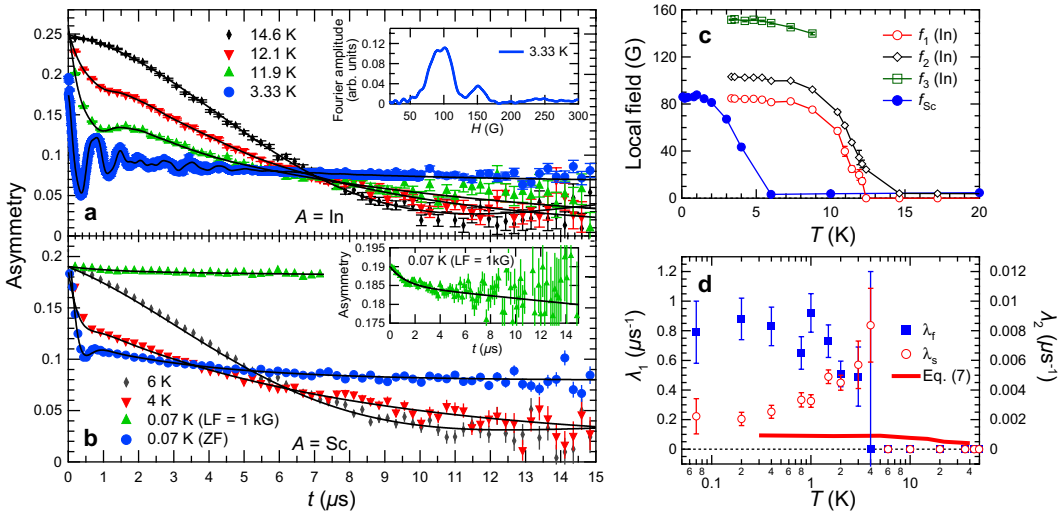

Figure 2. ZF- and LF-μSR results on $Li_2AMo_3O_8$. μSR time spectra of (**a**) $Li_2InMo_3O_8$ and (**b**) $Li_2ScMo_3O_8$. Solid lines in each panel represent the fitting curves (see the main text). A Fourier transform of the μSR time spectrum of $Li_2InMo_3O_8$ at 3.33 K (real amplitude) is plotted in the inset of (**a**). The inset of (**b**) shows a magnified view of the spectrum of $Li_2ScMo_3O_8$ at 0.07 K under $H_{LF} = 1$ kG. (**c**) Temperature dependences of local fields in $Li_2InMo_3O_8$ and $Li_2ScMo_3O_8$. (**d**) Temperature dependences of muon relaxation rates λ_f (left scale) and λ_s (right scale) of $Li_2ScMo_3O_8$ under longitudinal field. Solid line is calculated λ (right scale) using Eq. (7).

In the meanwhile, ZF-μSR time spectrum of $Li_2ScMo_3O_8$ at 0.07 K shows a highly damped oscillation with a pronounced reduction of the 1/3 tail as described in Fig. 2(b). To see the temperature evolution of the local fields in $Li_2ScMo_3O_8$, the ZF-μSR spectrum are fitted by combination of transverse and longitudinal relaxations

$$A_{ZF}(t) = A_1 \cos(2\pi f_{Sc} t + \phi)\exp(-\lambda_t t) + A_2 \exp(-\lambda_l t) + A_{BG}. \quad (2)$$

The fitting result at each temperature is plotted in Fig. 2(b), and temperature dependence of the local field f_{Sc} is also plotted in Fig. 2(c). One can clearly see the temperature evolution of f_{Sc} below 4 K with the critical exponent $\beta \sim 0.28$ which is similar to those of $Li_2InMo_3O_8$. Therefore, magnetic nature of these compounds are essentially the same, but it should be noted that the ground state of $Li_2ScMo_3O_8$ is short-range magnetic order by considering the strong damping of the oscillation below 4 K. The anomaly at 4 K was also found in the temperature derivative of the magnetic susceptibility[37]. Although the short-range magnetic order develops in $Li_2ScMo_3O_8$ below 4 K, the spectrum shows a moderate tail over a long period of time, suggesting that spin fluctuation survives even at 0.07 K. To explicitly distinguish the spin fluctuation of the Mo_3O_{13} cluster, we performed longitudinal field- (LF-) μSR measurements on $Li_2ScMo_3O_8$ under longitudinal magnetic field (H_{LF}) of 1 kG. Figure 2(b) and its inset display a LF-μSR time spectrum measured at 0.07 K. $H_{LF} = 1$ kG seems to be sufficient to quench (decouple) muon spin relaxations by both nuclear dipoles and the short-range ordered state. The characteristic LF-μSR spectrum of $Li_2ScMo_3O_8$ at 0.07 K was fitted by the following equation

$$A_{LF}(t) = A_f \exp(-\lambda_f t) + A_s \exp(-\lambda_s t) + A_{BG} \quad (3)$$

where A_f and A_s are asymmetries of fast (λ_f) and slow (λ_s) relaxation components, respectively ($A_f + A_s = 0.16$), and A_{BG} is the background asymmetry ($A_{BG} = 0.03$). The fitting results are described by the solid lines in Fig. 2(b) and its inset. We also fit LF-μSR time spectra under $H_{LF} = 1$ kG at several temperatures, and obtained temperature dependences of λ_f and λ_s are plotted in Fig. 2(d). λ_f shows a rapid relaxation with relative signal amplitude of ~3%. It mainly corresponds to the remnant signal from the short-range ordered state since λ_f exhibits a steep increase at 4 K as temperature goes down. On the other hand, λ_s shows a slow relaxation with two orders of magnitude less than λ_f, which is related to the intrinsic spin fluctuation of the Mo_3O_{13} cluster. Remarkably, temperature dependence of λ_s shows a temperature-independent plateau below 1 K and converges into the finite value of ~0.002 μs^{-1} which is very close to that of triangular lattice QSL 1T-TaS_2 ($\lambda = 0.0023\ \mu s^{-1}$ at 0.07 K)[23]. Indeed, such low-temperature plateau behaviors of muon relaxation rate is common feature in the TLHAF QSL candidates[20,25], which will be discussed again. To obtain complementary information to our μSR results on $Li_2AMo_3O_8$, TOF neutron scattering measurements were also conducted.

Elastic neutron scattering spectra of $Li_2InMo_3O_8$ below and above T_N are shown in Fig. 3(e). A magnetic Bragg peak appears at momentum transfer $Q = 0.719(1)$ Å^{-1} below T_N. The Q position corresponds to (1/3, 1/3, 0), indicating the 120° magnetic structure consistent with the previous ^{7}Li-NMR measurements[37]. By comparing the intensity of the magnetic peak with those of nuclear Bragg peaks, the ordered moment at 4.6 K is estimated to be 0.51(3) μ_B. Theoretically, the magnetic moment is reduced by about 59% for the spin-1/2 TLHAF[6], which is close to the observed ordered moment (reduced by 49% assuming $g = 2$). The reduced moment originates in a combination of geometrical frustration and quantum fluctuation. Neutron scattering intensity (I) map from $Li_2InMo_3O_8$ as a function of Q and energy transfer ($\hbar\omega$) at 4.5 K ($< T_N$) is shown in Fig. 3(a). Dispersive excitation centered at

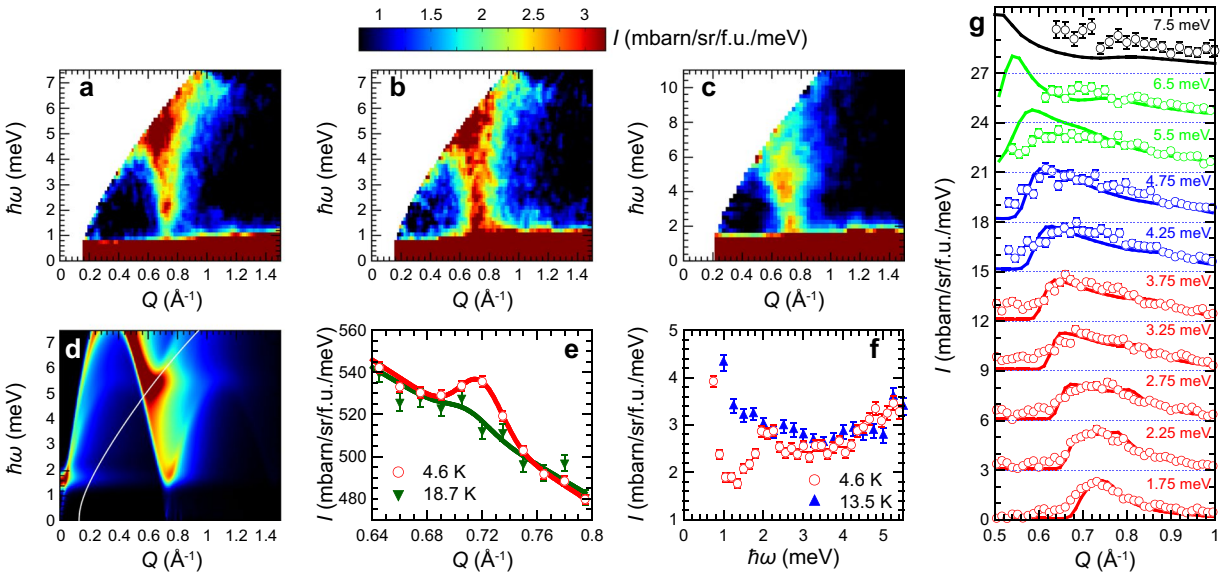

Figure 3. TOF neutron scattering results on $Li_2InMo_3O_8$. Low-energy inelastic neutron scattering intensity maps at (**a**) 4.6 K and (**b**) 13.5 K measured with $E_i = 11.9$ meV. (**c**) High-energy inelastic neutron scattering intensity map at 4.6 K measured with $E_i = 22.0$ meV. (**d**) Calculated inelastic neutron scattering intensity map at 4.6 K using the optimum parameters as described in the main text. Calculated energy resolution for $E_i = 11.9$ meV was convoluted. (**e**) Elastic neutron scattering intensities at 4.6 and 18.7 K with energy window of [−0.15, 0.15] meV. Solid lines represent the fitting result using the Gaussian function with linear background. (**f**) Energy spectra integrated over $Q = [0.69, 0.77]$ Å^{-1} at 4.6 and 13.5 K measured with $E_i = 11.9$ meV. (**g**) Q dependences of the neutron scattering intensities at several energy windows. Each energy window was [1.5, 2.0], [2.0, 2.5], [2.5, 3.0], [3.0, 3.5], and [3.5, 4.0] meV with $E_i = 11.9$ meV (red), [4.0, 4.5] and [4.5, 5.0] meV with $E_i = 15.8$ meV (blue), [5.0, 6.0] and [6.0, 7.0] meV with $E_i = 22.0$ meV (green), and [7.0, 8.0] meV with $E_i = 32.7$ meV (black), respectively. Constant background was subtracted from each Q dependence. Solid lines are calculated results using the optimum parameters in Eq. (5).

the magnetic zone center (1/3, 1/3, 0) was observed. Because of the Q position, the excitation is assigned to be the spin wave excitation in the long-range magnetic ordered state. Energy spectrum at the magnetic zone center exhibits a substantial peak at $\hbar\omega = 2.08(3)$ meV as shown in Fig. 3(f). This result claims that one branch (or some branches) of the spin wave excitation has spin gap at the magnetic zone center due to the magnetic anisotropy. On the other hand, magnetic signals at the magnetic zone center become quasielastic above T_N as shown in Fig. 3(b,f). Therefore, the gap-like excitation is a characteristic feature of the long-range magnetic ordered state. To observe the whole structure of the spin wave excitation at 4.5 K, $I(Q, \hbar\omega)$ map using higher E_i is presented in Fig. 3(c). The spin wave excitation survives up to ~9 meV. Q dependences of the spin wave intensities at various $\hbar\omega$s are plotted in Fig. 3(g). The spectra are asymmetric at $\hbar\omega > 3.0$ meV, and the peak shifts to lower Q at higher $\hbar\omega$. This result suggests that the squared magnetic form factor ($|F(Q)|^2$) of the Mo_3O_{13} cluster decreases quickly and is negligible at high Q, representing the unpaired electron with equal contributions from all three Mo atoms in $Li_2InMo_3O_8$.

For quantitative analysis on the spin wave excitation in $Li_2InMo_3O_8$, semi-classical linear spin wave (LSW) analysis was performed considering the 120° spin structure on the spin-1/2 2D Mo_3O_{13}-based triangular lattice [Fig. 1(c)]. The gap-like excitation at the magnetic zone center in the long-range magnetic ordered state is also observed in the other spin-1/2 triangular lattice system $Ba_3CoSb_2O_9$[13], and the peak energy (E_0) roughly scales with T_N in these compounds: $E_0 = 0.65$ meV and $T_N = 3.8$ K in $Ba_3CoSb_2O_9$[13] whereas $E_0 = 2.08$ meV and $T_N = 12$ K in $Li_2InMo_3O_8$. This suggests that the origin of the gap-like excitation in $Li_2InMo_3O_8$ is the same as that in $Ba_3CoSb_2O_9$[13]. Therefore, as in $Ba_3CoSb_2O_9$[12–14], the nearest-neighbor anisotropic exchange interaction was considered as the model Hamiltonian for $Li_2InMo_3O_8$

$$\mathcal{H} = \alpha J \sum_{i,j} (S_i^x S_j^x + S_i^y S_j^y + \delta S_i^z S_j^z) \tag{4}$$

where α, J, and δ represent the renormalization factor, the nearest neighbor exchange coupling constant, and the anisotropic factor. J was fixed to 112 K determined by the magnetic susceptibility measurement[37]. By fitting the calculated powder-averaged Q dependences to the experimental results at different $\hbar\omega$s (2~7.5 meV) simultaneously, optimum parameters were yielded

$$\begin{aligned} \alpha &= 0.56(1), \\ \delta &= 0.975(1). \end{aligned} \tag{5}$$

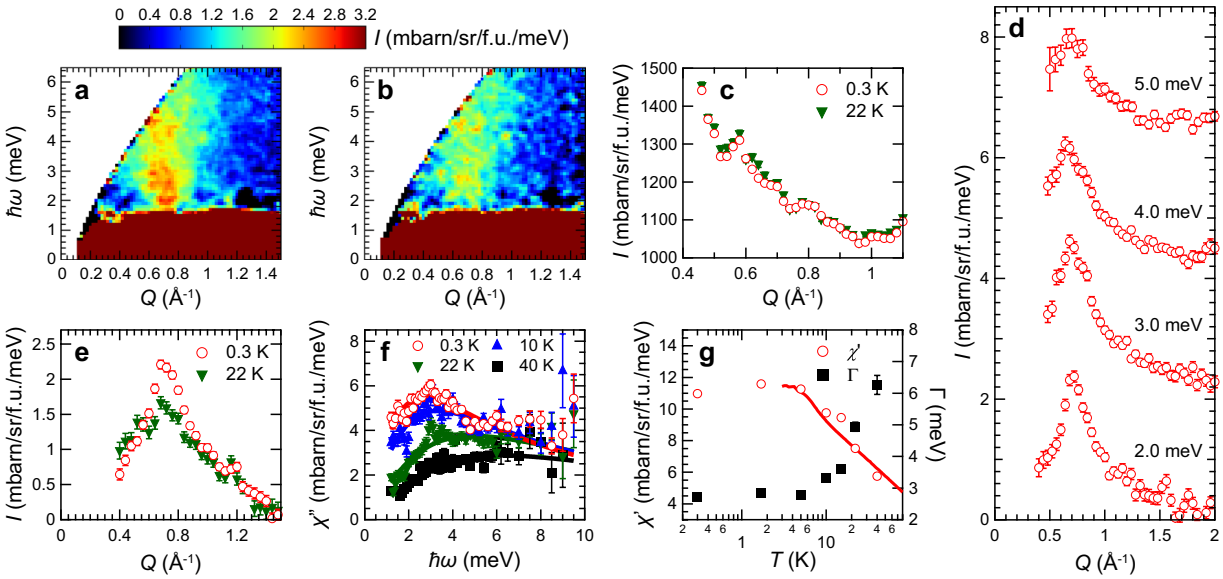

Figure 4. TOF neutron scattering results on $Li_2ScMo_3O_8$. Inelastic neutron scattering intensity maps with $E_i = 10.3$ meV measured at (**a**) 0.3 K and (**b**) 22 K. (**c**) Elastic neutron scattering intensities with energy window of [−0.075, 0.075] meV at 0.3 and 22 K with $E_i = 10.3$ meV. (**d**) Q dependences of the neutron scattering intensities at several energy windows at 1.7 K. Each energy window was [1.5, 2.5] meV with $E_i = 7.5$ meV, [2.5, 3.5] meV with $E_i = 10.3$ meV, [3.5, 4.5] meV with $E_i = 15.0$ meV, and [4.5, 5.5] meV with $E_i = 23.9$ meV, respectively. (**e**) Q dependences of the neutron scattering intensities with [1.5, 2.5] meV at 0.3 and 22 K using $E_i = 7.5$ meV. (**f**) Dynamical spin susceptibilities at $Q = [0.6, 0.8]$ Å^{-1} for 0.3, 10, 22, and 40 K. Solid lines are the fitting results by the quasielastic Lorentzian as described in the main text. (**g**) Temperature dependences of static spin susceptibility χ' (left scale) and relaxation rate Γ (right scale) obtained by the fitting in panel (f). Solid line is a scaled bulk magnetic susceptibility ($\chi_{bulk} = M/H$) measured with $H = 1$ T.

Fitting results together with the experimental results are shown in Fig. 3(g), and calculated LSW $I(Q, \hbar\omega)$ map is also shown in Fig. 3(d). Satisfactory agreements with calculation and experiment were confirmed. Obtained α is smaller than 1, indicating a negative quantum renormalization effect theoretically proposed for 2D spin-1/2 TLHAF[42–44]. Similar negative quantum renormalization effect ($\alpha \sim 0.65$) was also reported in $Ba_3CoSb_2O_9$[14]. Therefore, observed magnetic excitations of $Li_2InMo_3O_8$ in the accessible $(Q, \hbar\omega)$ region are well understood by the semi-classical LSW theory assuming the 120° magnetic structure on the spin-1/2 Mo_3O_{13} triangular lattice.

In contrast to $Li_2InMo_3O_8$, no magnetic Bragg peak evolves in the elastic channel down to 0.3 K in $Li_2ScMo_3O_8$ as plotted in Fig. 4(c), in agreement with our μSR results. On the other hand, diffuse scattering expected for the short-range order is not observed in our neutron measurements. Strong incoherent scattering may smear out such magnetic diffuse scattering in $Li_2ScMo_3O_8$. Figure 4(a) depicts $I(Q, \hbar\omega)$ map at 0.3 K. Clear diffuse scattering was observed in the inelastic channel. Although both magnetic excitations in $Li_2InMo_3O_8$ and $Li_2ScMo_3O_8$ are centered at $Q \sim 0.7$ Å^{-1} [Figs 3(a) and 4(a)], the overall structures are different, representing their different ground states. In $Li_2ScMo_3O_8$, steep continuum excitation was observed. The Q dependences of the magnetic excitations are invariant in the different energy windows as shown in Fig. 4(d). Steep continuum excitation, or spinon continuum, is the common feature of the magnetic excitations in the QSL candidates[3,21,22,26,45]. $I(Q, \hbar\omega)$ map at high temperature (22 K) is also shown in Fig. 4(b). Although overall magnetic fluctuation at 22 K is similar to that at 0.3 K, there are some differences. Scattering intensity decreases at 22 K. In addition, as shown in Fig. 4(e), spectrum weight of the Q dependence at 2 meV slightly shifts to $Q = 0$ at high temperature, which is also observed in other QSL candidates[22,26,45].

To investigate in more detail the characteristic energy (or time) scale of the steep continuum in $Li_2ScMo_3O_8$, the dynamical spin susceptibilities $\chi''(\hbar\omega) = [1 - \exp(-\hbar\omega/k_BT)]/|F(Q)|^2 I(\hbar\omega)$ at $Q = [0.6, 0.8]$ Å^{-1} where the magnetic signal is maximal are plotted for different temperatures in Fig. 4(f). The spectra are well fitted by the quasielastic Lorentzian $\chi''(\hbar\omega) = \chi'\hbar\omega\Gamma/[(\hbar\omega)^2 + \Gamma^2]$ where χ' is the static susceptibility and Γ the spin relaxation rate [or peak position of $\chi''(\hbar\omega)$]. The temperature dependences of the resulting parameters are shown in Fig. 4(g). Upon decreasing temperature, Γ decreases while χ' increases. Contrary to the conventional long-range ordered magnets, no divergent behavior was observed in the temperature dependences of χ' and Γ. It should be noted that χ' scales with bulk magnetic susceptibility χ_{bulk} over the temperature range of $3 \le T \le 40$ K [see solid line in Fig. 4(g)] and Γ is also scaled by the muon relaxation rate λ_s as discussed below. These fittings also extract two important features of the steep continuum in $Li_2ScMo_3O_8$: (1) the magnetic excitation is gapless consistent with the heat capacity measurement[37] and (2) the dynamical spin susceptibility extends from the elastic channel up to at least 9.5 meV which is about 1.6 J where J (=67 K) is determined by the magnetic susceptibility measurement[37].

Complementary analysis of μSR and INS results enables us to exclusively clarify the quantum fluctuations in $Li_2ScMo_3O_8$. Muon spin relaxation rate λ_s in Fig. 2(d) is related to the spin relaxation rate of the magnetic fluctuation Γ in Fig. 4(g) on the basis of following Redfield's formula[46]

$$\lambda = \frac{2(\gamma_\mu \delta_\mu)^2 \Gamma}{(\gamma_\mu H_{LF})^2 + \Gamma^2} \tag{6}$$

where γ_μ and δ_μ are the gyromagnetic ratio of muon ($=2\pi \times 135.54$ MHz/T) and average distribution of local magnetic fields at muon sites. We performed electrostatic potential calculations using a point-charge model[47] and estimated $\delta_\mu = 204.8$ G for $Li_2ScMo_3O_8$ (see Supplementary Information). Since H_{LF} ($=1$ kG $= 8.5 \times 10^8$ Hz) is much smaller than Γ ($=2.7$ meV $= 6.5 \times 10^{11}$ Hz at 0.3 K) in $Li_2ScMo_3O_8$, Eq. (6) is reformulated as

$$\lambda \sim \frac{2(\gamma_\mu \delta_\mu)^2}{\Gamma}. \tag{7}$$

We plotted calculated temperature dependence of λ using Γ obtained by our INS measurements and compared with λ_s obtained by our LF-μSR measurements [see solid line for calculation and circles for μSR results in Fig. 2(d)]. Quantitative agreement can be seen; the anomaly around 4 K is artificial feature owing to λ_f. Therefore, both μSR and INS measurements exhibit that quantum fluctuations persist at the lowest measured temperature. As mentioned above, such low-temperature plateaus of the relaxation rates were widely observed in the triangular-lattice[20,25] and kagome-lattice[45,48–51] QSL candidates.

To account for the QSL-like excitations in $Li_2ScMo_3O_8$, we now consider the spinon Fermi surface QSL model. In $Li_2ScMo_3O_8$, no static long-range order was detected even down to 0.07 K [Figs 2(b) and 4(c)]. Alternatively, gapless continuum in $Li_2ScMo_3O_8$ was observed at $Q = 0.726(4)$ Å^{-1} corresponding to the (1/3, 1/3, 0) position [Fig. 4(a,d,f)]. Moreover, both λ_s and Γ exhibit temperature-independent plateaus at low temperature [Figs 2(d) and 4(g)]. These features are well explained by QSL with spinon Fermi surface[27,28]. As discussed in earlier works[20,21,26], the spinon Fermi surface QSL model on the spin-1/2 TLHAF expects that (1) absence of static long-range magnetic order, (2) muon spin relaxation rate approach a finite value as temperature approaches zero, (3) magnetic excitation is gapless continuum, and (4) $\chi''(Q, \hbar\omega)$ shows the maximum intensity at the corner of the 2D Brillouin zone [e.g. (1/3, 1/3, 0)]. All observed features of the magnetic fluctuation in $Li_2ScMo_3O_8$ can be well described by the spinon Fermi surface QSL model. Although the second peak of the spinon continuum in $Ba_3NiSb_2O_9$ was also observed at (2/3, 2/3, 0)[26], the second peak in $Li_2ScMo_3O_8$ was not detected at (2/3, 2/3, 0) corresponding to $Q = 1.45$ Å^{-1} as shown in Fig. 4(d) because of the quick decay of the squared magnetic form factor of the Mo_3O_{13} cluster[33]. By performing complementary analysis on μSR and INS results, we conclude that $Li_2ScMo_3O_8$ undergoes the short-range magnetic order below 4 K with the QSL-like fluctuations which persist down to the lowest temperature.

We compare the Mo_3O_{13}-cluster-based triangular lattice antiferromagnets, $Li_2AMo_3O_8$ and $LiZn_2Mo_3O_8$, in line with the recent theory by Chen *et al.*[35]. They proposed a 1/6-filled Hubbard model on an anisotropic kagome lattice with the nearest-neighbor electron hopping and repulsions[35] to account for the magnetism in $LiZn_2Mo_3O_8$[29]. Electron is fractionalized into charged boson and spin-carring spinons; plaquette charge order emerges as the charge ground state and the spin degree of freedom can be then described by $U(1)$ QSL with spinon Fermi surface, which can explain the unusual magnetic susceptibility in $LiZn_2Mo_3O_8$[29]. For comparison with different compounds, they introduce a phenomenological parameter ξ to characterize the anisotropy of the Mo kagome lattice: $\xi = d_{inter}/d_{intra}$ where d_{intra} (d_{inter}) is the intracluster (intercluster) Mo-Mo bond length. Large anisotropy ξ tends to suppress charge fluctuations between clusters leading to the 120° long-range magnetic order whereas small anisotropy ξ corresponds to large charge fluctuation generating the $U(1)$ QSL with spinon Fermi surface. Using the structural parameters summarized in Supplementary Information, we estimated ξ as 1.271, 1.269, and 1.258 for $Li_2InMo_3O_8$, $Li_2ScMo_3O_8$, and $LiZn_2Mo_3O_8$[29], respectively. The phenomenological parameter ξ explains the different ground states between the 120° long-range magnetic order in $Li_2InMo_3O_8$ and the condensed VBS in $LiZn_2Mo_3O_8$. However, the ξ values of $Li_2InMo_3O_8$ and $Li_2ScMo_3O_8$ are very close to each other in spite of their different ground states. Nevertheless, ^{115}In and ^{45}Sc NMR measurements on $Li_2AMo_3O_8$ reported that charge fluctuation in $Li_2ScMo_3O_8$ is 2.6 times larger than that in $Li_2InMo_3O_8$[52], and the difference between charge fluctuations can qualitatively explain the different ground states of $Li_2InMo_3O_8$ and $Li_2ScMo_3O_8$. Therefore, the anisotropic parameter for the Mo kagome lattice, ξ, is too simplified to explain the different ground states in $Li_2AMo_3O_8$, and more detailed parameter is required for $Li_2AMo_3O_8$.

We also compare the magnetic excitations in $Li_2InMo_3O_8$ and $Li_2ScMo_3O_8$ to discuss the origin of the different ground states. Although both magnetic excitations in $Li_2InMo_3O_8$ and $Li_2ScMo_3O_8$ center at $Q \sim 0.72$ Å^{-1}, low-energy magnetic excitations show opposite behaviors. The magnetic excitation at the magnetic zone center in $Li_2InMo_3O_8$ clearly exhibits the peak at 2.08(3) meV [Fig. 3(a,f)]. Our LSW analysis suggests that the anisotropic exchange interaction is necessary to reproduce the peak. Meanwhile, the gapless magnetic excitation in $Li_2ScMo_3O_8$ indicates that magnetic anisotropy is negligibly small in $Li_2ScMo_3O_8$ [Fig. 4(a,f)]. Thus, the difference in the magnetic anisotropy is another possibility of the origin of the different ground states in $Li_2AMo_3O_8$. In fact, the gap-like excitation was observed in the long-range ordered state of $Ba_3CoSb_2O_9$[13,14], whereas the gapless magnetic excitations in the QSL systems $YbMgGaO_4$[21,22] and $Ba_3NiSb_2O_9$[26]. INS measurements on magnetic excitations in the substitution system $Li_2(In_{1-x}Sc_x)Mo_3O_8$[40] are effective to further elucidate the origin of different magnetic ground states, which is left for future work.

Conclusion

We performed a comprehensive study on the quantum magnetisms in the Mo_3O_{13}-cluster-based spin-1/2 triangular lattice antiferromagnets, $Li_2InMo_3O_8$ and $Li_2ScMo_3O_8$ by means of μSR and TOF neutron scattering techniques. Spin wave excitation in $Li_2InMo_3O_8$ was well described by the nearest neighbor anisotropic Heisenberg model based on the 120° spin structure. $Li_2ScMo_3O_8$ exhibits the short-range magnetic order below 4 K with the QSL-like fluctuations which persist down to the lowest temperature. The origin of the different magnetic ground states in $Li_2AMo_3O_8$ is discussed in terms of anisotropies of crystal structures and magnetic interactions.

Methods

The preparation of polycrystalline $Li_2InMo_30_8$ ($Li_2ScMo_3O_8$) was carried out by two steps[37]. First, to synthesize a precursor Li_2MoO_4, a mixture with a ratio of MoO_3:$Li_2CO_3 = 1{:}1$ was ground, placed in an alumina crucible, and heated at 873 K for 24 hours in air; we repeated this step for three times. Then, a mixture having a ratio of In_2O_3 (Sc_2O_3):Li_2MoO_4:MoO_3:Mo = 0.5:1:0.84:1.16 was ground, pressed into a pellet, sealed in an evacuated quartz tube, heated at 923 K for 12 hours, and heated at 1198 K (1173 K) for 24 hours; we repeated this step for two times. Magnetization measurements were performed using a commercial superconducting quantum interference device (SQUID) magnetometer (Quantum Design Magnetic Property Measurement System, MPMS). ZF- and LF-μSR experiments were performed using the Advanced Research Targeted Experimental Muon Instrument at the S1 line spectrometer (ARTEMIS)[53] with a conventional ^{4}He flow cryostat and the D1 spectrometer[53] with a ^{3}He-^{4}He dilution refrigerator installed at Materials and Life Science Experimental Facility (MLF), Japan Proton Accelerator Research Complex (J-PARC). We used the VASP software[54] for DFT calculation and the DipElec program[47] to calculate the local magnetic fields in $Li_2ScMo_3O_8$. TOF neutron scattering measurements were performed using the Fermi chopper spectrometer 4SEASONS at MLF, J-PARC[55]. Frequencies of the Fermi chopper were 350 and 250 Hz for the In and Sc systems, resulting in the combinations of incident neutron energies of 11.9, 15.8, 22.0, and 32.7 meV, and 7.5, 10.3, 15.0, and 23.9 meV[56], respectively. A standard top-loading cryostat at 4SEASONS was used for the measurements on $Li_2InMo_3O_8$, whereas a ^{4}He refrigerator and a ^{3}He cryostat were used for $Li_2ScMo_3O_8$. Empty can was measured at corresponding temperatures, and then subtracted from raw data of $Li_2ScMo_3O_8$. TOF data were visualized by software suite Utsusemi[57]. Neutron scattering intensities are converted to the absolute unit using the incoherent scattering of each sample[58] after correction of the neutron absorption effect. Squared magnetic form factor of the Mo_3O_{13} cluster[33] and $\hbar\omega$-dependent energy resolution at 4SEASONS[59] were included in the LSW calculations for $Li_2InMo_3O_8$.

Data Availability

The datasets generated and analyzed during the current study are available from the corresponding author.

References

1. Balents, L. Spin liquids in frustrated magnets. *Nature* **464**, 199–208 (2010).
2. Savary, L. & Balents, L. Quantum spin liquids: a review. *Rep. Prog. Phys.* **80**, 016502 (2017).
3. Han, T.-H. *et al*. Fractionalized excitations in the spin-liquid state of a kagome-lattice antiferromagnet. *Nature* **492**, 406–410 (2012).
4. Seabra, L., Momoi, T., Sindzingre, P. & Shannon, N. Phase diagram of the classical Heisenberg antiferromagnet on a triangular lattice in an applied magnetic field. *Phys. Rev. B* **84**, 214418 (2011).
5. Huse, D. A. & Elser, V. Simple variational wave functions for two-dimensional Heisenberg spin-1/2 antiferromagnets. *Phys. Rev. Lett.* **60**, 2531–2534 (1988).
6. Capriotti, L., Trumper, A. E. & Sorella, S. Long-range Néel order in triangular Heisenberg model. *Phys. Rev. Lett.* **82**, 3899–3902 (1999).
7. White, S. R. & Chernyshev, A. L. Néel order in square and triangular lattice Heisenberg models. *Phys. Rev. Lett.* **99**, 127004 (2007).
8. Iqbal, Y., Hu, W.-J., Thomale, R., Poilblanc, D. & Becca, F. Spin liquid nature in the Heisenberg J_1–J_2 triangular antiferromagnet. *Phys. Rev. B* **93**, 144411 (2016).
9. Motrunich, O. I. Variational study of triangular spin-1/2 model with ring exchanges and spin liquid state in κ-$(ET)_2Cu_2(CN)_3$. *Phys. Rev. B* **72**, 045105 (2005).
10. Trumper, A. E. Spin-wave analysis to the spatially anisotropic Heisenberg antiferromagnet on a triangular lattice. *Phys. Rev. B* **72**, 2987–2989 (1999).
11. Watanabe, K., Kawamura, H., Nakano, H. & Sakai, T. Quantum spin-liquid behavior in the spin-1/2 random Heisenberg antiferromagnet on the triangular lattice. *J. Phys. Soc. Jpn.* **83**, 034714 (2014).
12. Shirata, Y., Tanaka, H., Matsuo, A. & Kindo, K. Experimental realization of a spin-1/2 triangular-lattice Heisenberg antiferromagnet. *Phys. Rev. Lett.* **108**, 057205 (2012).
13. Ma, J. *et al*. Static and dynamical properties of the spin-1/2 equilateral triangular-lattice antiferromagnet $Ba_3CoSb_2O_9$. *Phys. Rev. Lett.* **116**, 087201 (2016).
14. Ito, S. *et al*. Structure of the magnetic excitations in the spin-1/2 triangular-lattice Heisenberg antiferromagnet $Ba_3CoSb_2O_9$. *Nat. Commun.* **8**, 235 (2017).
15. Shimizu, Y., Miyagawa, K., Kanoda, K., Maesato, M. & Saito, G. Spin liquid state in an organic Mott insulator with a triangular lattice. *Phys. Rev. Lett.* **91**, 107001 (2003).
16. Yamashita, S. *et al*. Thermodynamic properties of a spin-1/2 spin-liquid state in a κ-type organic salt. *Nat. Phys.* **4**, 459–462 (2008).
17. Yamashita, M. *et al*. Highly mobile gapless excitations in a two-dimensional candidate quantum spin liquid. *Science* **328**, 1246–1248 (2010).
18. Yamashita, S., Yamamoto, T., Nakazawa, Y., Tamura, M. & Kato, R. Gapless spin liquid of an organic triangular compound evidenced by thermodynamic measurements. *Nat. Commun.* **2**, 275 (2011).
19. Li, Y. *et al*. Gapless quantum spin liquid ground state in the two-dimensional spin-1/2 triangular antiferromagnet $YbMgGaO_4$. *Sci. Rep.* **5**, 16419 (2015).
20. Li, Y. *et al*. Muon spin relaxation evidence for the U(1) quantum spin-liquid ground state in the triangular antiferromagnet $YbMgGaO_4$. *Phys. Rev. Lett.* **117**, 097201 (2016).
21. Shen, Y. *et al*. Evidence for a spinon Fermi surface in a triangular-lattice quantum-spin-liquid candidate. *Nature* **540**, 559–562 (2016).
22. Paddison, J. A. M. *et al*. Continuous excitations of the triangular-lattice quantum spin liquid $YbMgGaO_4$. *Nat. Phys.* **13**, 117–122 (2017).
23. Klanjšek, M. *et al*. A high-temperature quantum spin liquid with polaron spins. *Nat. Phys.* **13**, 1130–1134 (2017).

24. Cheng, J. G. *et al*. High-pressure sequence of $Ba_3NiSb_2O_9$ structural phases: new $S = 1$ quantum spin liquids based on Ni^{2+}. *Phys. Rev. Lett.* **107**, 197204 (2011).
25. Quilliam, J. A. *et al*. Gapless quantum spin liquid ground state in the spin-1 antiferromagnet 6HB-$Ba_3NiSb_2O_9$. *Phys. Rev. B* **93**, 214432 (2016).
26. Fåk, B. *et al*. Evidence for a spinon Fermi surface in the triangular $S = 1$ quantum spin liquid $Ba_3NiSb_2O_9$. *Phys. Rev. B* **95**, 060402(R) (2017).
27. Lee, S.-S. & Lee, P. A. U(1) gauge theory of the Hubbard model: spin liquid states and possible application to κ-(BEDT-TTF)$_2$Cu$_2$(CN)$_3$. *Phys. Rev. Lett.* **95**, 036403 (2005).
28. Norman, M. R. & Micklitz, T. How to measure a spinon Fermi surface. *Phys. Rev. Lett.* **102**, 067204 (2009).
29. Sheckelton, J. P., Neilson, J. R., Soltan, D. G. & McQueen, T. M. Possible valence-bond condensation in the frustrated cluster magnet $LiZn_2Mo_3O_8$. *Nat. Mater.* **11**, 493–496 (2012).
30. Anderson, P. W. Resonating valence bonds: a new kind of insulator? *Mater. Res. Bull.* **8**, 153–160 (1973).
31. Fazekas, P. & Anderson, P. W. On the ground state properties of the anisotropic triangular antiferromagnet. *Phil. Mag.* **30**, 423–440 (1973).
32. Sheckelton, J. P. *et al*. Local magnetism and spin correlations in the geometrically frustrated cluster magnet $LiZn_2Mo_3O_8$. *Phys. Rev. B* **89**, 064407 (2014).
33. Mourigal, M. *et al*. Molecular quantum magnetism in $LiZn_2Mo_3O_8$. *Phys. Rev. Lett.* **112**, 027202 (2014).
34. Flint, R. & Lee, P. A. Emergent honeycomb lattice in $LiZn_2Mo_3O_8$. *Phys. Rev. Lett.* **111**, 217201 (2013).
35. Chen, G., Kee, H.-Y. & Kim, Y. B. Cluster Mott insulators and two Curie-Weiss regimes on an anisotropic kagome lattice. *Phys. Rev. B* **93**, 245134 (2016).
36. Gall, P., Orabi, R. A. R. A., Guizouarn, T. & Gougeon, P. Synthesis, crystal structure and magnetic properties of $Li_2InMo_3O_8$: a novel reduced molybdenum oxide containing magnetic Mo_3 clusters. *J. Solid State Chem.* **208**, 99 (2013).
37. Haraguchi, Y., Michioka, C., Imai, M., Ueda, H. & Yoshimura, K. Spin-liquid behavior in the spin-frustrated Mo_3 cluster magnet $Li_2ScMo_3O_8$ in contrast to magnetic ordering in isomorphic $Li_2InMo_3O_8$. *Phys. Rev. B* **92**, 014409 (2015).
38. Zhou, H. D. *et al*. Spin liquid state in the $S = 1/2$ triangular lattice $Ba_3CuSb_2O_9$. *Phys. Rev. Lett.* **106**, 147204 (2011).
39. Sugiyama, J. *et al*. Internal magnetic field on the two-dimensional triangular lattice formed by Mo_3O_8 trimers. *J. Phys.: Conf. Ser.* **21**, 011012 (2018).
40. Akbari-Sharbaf, A. *et al*. Tunable quantum spin liquidity in the 1/6th-filled breathing kagome lattice. *Phys. Rev. Lett.* **120**, 227201 (2018).
41. Portis, A. M. & Celio, M. Muon and other studies of magnetic ordering in cuprate layer-compounds. *Hyperfine Interactions* **49**, 129–166 (1989).
42. Starykh, O. A., Chubukov, A. V. & Abanov, A. G. Flat spin-wave dispersion in a triangular antiferromagnet. *Phys. Rev. B* **74**, 180403(R) (2006).
43. Zheng, W., Fjarestand, J. O., Singh, R. R. P., McKenzie, R. H. & Coldea, R. Excitation spectra of the spin-1/2 triangular-lattice Heisenberg antiferromagnet. *Phys. Rev. B* **74**, 224420 (2006).
44. Chernyshev, A. L. & Zhitomirsky, M. E. Spin waves in a triangular lattice antiferromagnet: decays, spectrum renormalization, and singularities. *Phys. Rev. B* **79**, 144416 (2009).
45. Fåk, B. *et al*. Kapellasite: a kagome quantum spin liquid with competing interactions. *Phys. Rev. Lett.* **109**, 037208 (2012).
46. Slichter, C. P. *Principles of Magnetic Resonance*. 3rd edition, (Springer Verlag, New York, 1990).
47. Kojima, K. M. *et al*. Site-dilution in the quasi-one-dimensional antiferromagnet $Sr_2(Cu_{1-x}Pd_x)O_3$: reduction of Néel temperature and spatial distribution of ordered moment sizes. *Phys. Rev. B* **70**, 094402 (2004).
48. Mendels, P. *et al*. Quantum magnetism in the paratacamite family: towards an ideal kagomé lattice. *Phys. Rev. Lett.* **98**, 077204 (2007).
49. Kermarrec, E. *et al*. Spin-liquid ground state in the frustrated kagome antiferromagnet $MgCu_3(OH)_6Cl_2$. *Phys. Rev. B* **84**, 100401(R) (2011).
50. Clark, L. *et al*. Gapless spin liquid ground state in the $S = 1/2$ vanadium oxyfluoride kagome antiferromagnet $[NH_4]_2[C_7H_{14}N][V_7O_6F_{18}]$. *Phys. Rev. Lett.* **110**, 207208 (2013).
51. Gomilsek, M. *et al*. Instabilities of spin-liquid states in a quantum kagome antiferromagnet. *Phys. Rev. B* **93**, 060405(R) (2016).
52. Haraguchi, Y., Michioka, C., Ueda, H. & Yoshimura, K. Charge fluctuation in $S = 1/2$ triangular lattice cluster antiferromagnets $Li_2ScMo_3O_8$ and $Li_2InMo_3O_8$. *J. Phys.: Conf. Series* **868**, 012022 (2017).
53. Kojima, K. M. *et al*. New μSR spectrometer at J-PARC MUSE based on Kalliope detectors. *J. Phys. Conf. Ser.* **551**, 012063 (2014).
54. Kresse, G. & Hafner, J. Ab initio molecular dynamics for liquid metals. *Phys. Rev. B* **47**, 558–561 (1993).
55. Kajimoto, R. *et al*. The Fermi chopper spectrometer 4SEASONS at J-PARC. *J. Phys. Soc. Jpn.* **80**, SB025 (2011).
56. Nakamura, M. *et al*. First demonstration of novel method for inelastic neutron scattering measurement utilizing multiple incident energies. *J. Phys. Soc. Jpn.* **78**, 093002 (2009).
57. Inamura, Y., Nakatani, T., Suzuki, J. & Otomo, T. Development status of software "Utsusemi" for chopper spectrometers at MLF, J-PARC. *J. Phys. Soc. Jpn.* **82**, SA031 (2013).
58. Xu, G., Xu, Z. & Tranquada, J. M. Absolute cross-section normalization of magnetic neutron scattering data. *Rev. Sci. Instrum.* **84**, 083906 (2013).
59. Iida, K. *et al*. Energy- and Q-resolution investigations of a chopper spectrometer 4SEASONS at J-PARC. *JPS Conf. Proc.* **1**, 014016 (2014).

Acknowledgements

We thank Seiko Ohira-Kawamura and Kim Sandvik for helpful discussion and Hua Li for DFT calculations. We also acknowledge technical supports from the MLF sample environment team. Magnetic susceptibility measurements were performed at the CROSS user laboratories. The synchrotron X-ray diffraction experiments were conducted at BL5S2 of Aichi Synchrotron Radiation Center, Aichi Science and Technology Foundation, Aichi, Japan (Proposal Nos. 201803046 and 201803047). The μSR measurements at the S1 and D1 beamlines were conducted under the user program with proposal number 2017B0033. The proposal numbers for the TOF neutron scattering experiments at 4SEASONS were 2016I0001, 2017A0004, 2017B0030, and 2018I0001. The DFT calculations were supported by the Condensed Matter Research Center, Institute of Materials Structure Science, KEK, and the KEK Large Scale Simulation Program (Nos 15/16-07 and 16/17-18). This work was partially supported by JSPS KAKENHI Grant Numbers JP17K14349 and JP18K03529, and the Cooperative Research Program of "Network Joint Research Center for Materials and Devices" (20181072).

Author Contributions

K.I. designed the project. H.Y. and Y. Ishii synthesized the polycrystalline samples. H.Y., Y. Ishii, M.I. and K.I. characterized the samples. N.K. conducted synchrotron X-ray diffraction measurements and Rietveld analysis. H.O., A.K., R. Kadono, K.I. and R. Kajimoto conducted muon experiments while K.I., R. Kajimoto, H.Y., Y. Inamura, N.M. and M.I. performed neutron scattering measurements. K.I., H.O. and N.K. analyzed the data and wrote the manuscript. All authors discussed the results and commented on the manuscript.

Additional Information

Supplementary information accompanies this paper at https://doi.org/10.1038/s41598-018-36123-7.

Competing Interests: The authors declare no competing interests.

Publisher's note: Springer Nature remains neutral with regard to jurisdictional claims in published maps and institutional affiliations.